HEAT-TRANSFER INVESTIGATION OF LANGLEY RESEARCH CENTER DELTA WING CONFIGURATIONS AT MACH NUMBERS 8 AND 10.5

R. H. Eaves, Jr., et al

Arnold Engineering Development Center
Arnold Air Force Station, Tennessee

February 1973

AEDC-TR-72-196

HEAT-TRANSFER INVESTIGATION OF LANGLEY RESEARCH CENTER DELTA WING CONFIGURATIONS AT MACH NUMBERS 8 AND 10.5

R. H. Eaves, Jr., R. K. Matthews, and T. D. Buchanan

ARO, Inc.

February 1973

VON KÁRMÁN GAS DYNAMICS FACILITY
ARNOLD ENGINEERING DEVELOPMENT CENTER
AIR FORCE SYSTEMS COMMAND
ARNOLD AIR FORCE STATION, TENNESSEE

43
R

NOTICES

When U. S. Government drawings specifications, or other data are used for any purpose other than a definitely related Government procurement operation, the Government thereby incurs no responsibility nor any obligation whatsoever, and the fact that the Government may have formulated, furnished, or in any way supplied the said drawings, specifications, or other data, is not to be regarded by implication or otherwise, or in any manner licensing the holder or any other person or corporation, or conveying any rights or permission to manufacture, use, or sell any patented invention that may in any way be related thereto.

Qualified users may obtain copies of this report from the Defense Documentation Center.

References to named commercial products in this report are not to be considered in any sense as an endorsement of the product by the United States Air Force or the Government.

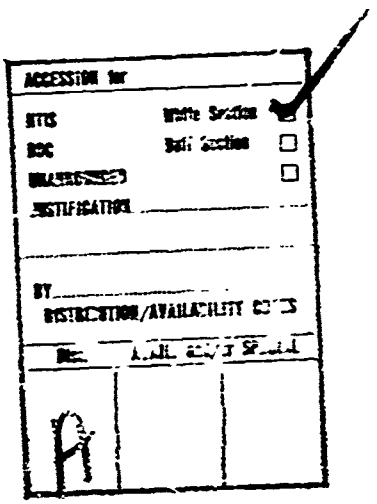

UNCLASSIFIED

Security Classification

DOCUMENT CONTROL DATA - R & D

(Security classification of title, body of abstract and indexing annotation must be entered when the overall report is classified)

1 ORIGINATING ACTIVITY (Corporate author) Arnold Engineering Development Center Arnold Air Force Station, Tennessee 37389	2a. REPORT SECURITY CLASSIFICATION UNCLASSIFIED 2b. GROUP N/A

3 REPORT TITLE

HEAT-TRANSFER INVESTIGATION OF LANGLEY RESEARCH CENTER DELTA WING CONFIGURATIONS AT MACH NUMBERS 8 AND 10.5

4 DESCRIPTIVE NOTES (Type of report and inclusive dates)

Final Report - June to September 1971

5 AUTHOR(S) (First name, middle initial, last name)

R. H. Eaves, Jr., R. K. Matthews, and T. D. Buchanan, ARO, Inc.

6 REPORT DATE	7a. TOTAL NO OF PAGES	7b. NO OF REFS
February 1973	43	28

8a CONTRACT OR GRANT NO b. PROJECT NO c. Program Element 921E-2 d.	9a. ORIGINATOR'S REPORT NUMBER(S) AEDC-TR-72-196 9b. OTHER REPORT NO(S) (Any other numbers that may be assigned this report) ARO-VKF-TR-72-160

10 DISTRIBUTION STATEMENT

Approved for public release; distribution unlimited.

11 SUPPLEMENTARY NOTES	12. SPONSORING MILITARY ACTIVITY
Available in DDC	NASA Marshall Space Flight Center A&E-AERO-AAE Huntsville, Alabama 35812

13 ABSTRACT

Heat-transfer tests for two simple delta wing configurations submitted by NASA-Langley Research Center (LRC) were conducted at Mach numbers 8 and 10.5. Test conditions provided both Mach number and Reynolds number simulation for typical lifting body reentry trajectories. This report presents the major test results and comparisons with theoretical calculations. Specific test results include heat-transfer distributions, shock angles, limited pressure measurements, and boundary-layer transition results.

DD FORM 1 NOV 68 1473

UNCLASSIFIED

Security Classification

14 KEY WORDS	LINK A		LINK B		LINK C	
	ROLE	WT	ROLE	WT	ROLE	WT
delta wings						
wing-body configurations						
hypersonic flow						
reentry trajectories						
heat transfer						
pressure distribution						
boundary layer transition						
wind tunnel tests						

HEAT-TRANSFER INVESTIGATION OF LANGLEY RESEARCH CENTER DELTA WING CONFIGURATIONS AT MACH NUMBERS 8 AND 10.5

R. H. Eaves, Jr., R. K. Matthews, and T. D. Buchanan
ARO, Inc.

FOREWORD

The work reported herein was conducted at the Arnold Engineering Development Center (AEDC) at the request of the Marshall Space Flight Center (NASA-MSFC), Huntsville, Alabama, under Program Element 921E-2.

The results of tests presented were obtained by ARO, Inc. (a subsidiary of Sverdrup & Parcel and Associates, Inc.), contract operator of AEDC, AFSC, Arnold Air Force Station, Tennessee. The tests were conducted in June and September, 1971 under ARO Project No. VT1162. The final data analysis was completed on May 10, 1972. The manuscript was submitted for publication on October 5, 1972.

The authors wish to express their appreciation to L. L. Trimmer, who was the Facility coordinator for these tests at AEDC. The assistance of H. R. Little and A. H. Boudreau, who helped on the Tunnel F test, is also acknowledged. Dr. J. C. Adams and W. R. Martindale are responsible for the theoretical solutions presented herein, and G. E. Gilley deserves recognition for his efforts in developing the phase-change paint data reduction program.

This technical report has been reviewed and is approved.

JIMMY W. MULLINS
Lt Colonel, USAF
Chief Air Force Test Director, VKF
Directorate of Test

A. L. COAPMAN
Colonel, USAF
Director of Test

CONTENTS

APPENDIXES

Figure | Page

NOMENCLATURE

c	Specific heat of phase-change paint models, Btu/lbm-°R
H_o	Stagnation enthalpy, Btu/lbm
h	Heat-transfer coefficient, $\dot{q}/(T_o - T_w)$, Btu/ft^2-sec-°R
k	Conductivity of phase-change paint models, Btu/ft-sec-°R
ℓ	Axial length of model, ℓ = 24 in.
M	Mach number
p	Pressure, psia
p'_o	Stagnation pressure downstream of a normal shock, psia
$\dot{q}$	Heat-transfer rate, Btu/ft^2-sec
Re	Unit Reynolds number, ft^{-1}
$Re_{e,\theta}$	Reynolds number based on edge conditions and momentum thickness at beginning of transition
$Re_{\infty,\ell}$	Free-stream Reynolds number based on length, ℓ
r_n	Model profile nose radius, 0.675 in.
T	Temperature, °F or °R as noted
Δt	Time increment that model has been exposed to uniform flow, sec
U	Free-stream velocity, ft/sec
x	Axial distance from model nose, in. (see Fig. 2)
y	Spanwise distance from model centerline, in. (see Fig. 2)
y_{max}	Local semispan at a given axial location, in. (see Fig. 2)
α	Angle of attack, deg
δ_s	Angle between local tangent to model surface and bow shock, deg
ρ	Density, lbm/ft^3

SUBSCRIPTS

aw	Adiabatic wall conditions
e	Edge conditions
i	Initial conditions
o	Stilling chamber conditions
pc	Phase change
ref	Heat-transfer parameter based on 0.675-in. nose radius $M_\infty = 8$ (Tunnel B), $\dot{q}_{ref}$ and h_{ref} based on Fay-Riddell Theory. $M_\infty \approx 10.5$ (Tunnel F), h_{ref} based on Fay-Riddell Theory and $\dot{q}_{ref}$ measured on a 0.5-in.-radius hemisphere cylinder and adjusted to a 0.675-in. radius.
w	Wall conditions
∞	Free-stream conditions

SECTION I
INTRODUCTION

In support of the Phase B design studies of the Space Transportation System (Space Shuttle), extensive aerothermodynamic tests of several proposed configurations sponsored by NASA-MSFC were conducted at the von Karman Facility of the AEDC. Briefly, these tests were to provide aerodynamic heating results for the booster and orbiter during launch and reentry for various model designs submitted by two Phase B contractor teams. In addition, tests of basic delta wing configurations supplied by NASA-LRC were included in the test program. All data generated during this test program were submitted to the NASA-sponsored "System for Automated Development of Static Aerothermodynamic Criteria" (SADSAC) and are documented in data reports (Refs. 1 through 16). Test results from booster and orbiter configurations from the Phase B contractor teams are summarized in two AEDC technical reports (Refs. 17 and 18). Test results from the delta wing configurations for NASA Langley Research Center are reported herein.

From a theoretical viewpoint it is desirable to analyze and understand the flow process for simple geometry shapes before analyzing the more complex space shuttle configurations. This report summarizes the aerodynamic heating on two relatively simple delta wing configurations provided by the Langley Research Center that should provide useful information for designing more complex configurations.

The objectives for the tests reported herein were as follows:

1. Provide turbulent heating data corresponding to the reentry trajectory of typical orbiter configurations.

2. Provide boundary-layer transition data at reentry conditions.

To accomplish these test objectives, two VKF test facilities, the continuous Hypersonic Wind Tunnel (B) and the hotshot-type Hypervelocity Wind Tunnel (F), were utilized. The tests were conducted in Tunnel B at Mach number 8 and in Tunnel F at an approximate Mach number 10.5 for angles of attack of 20, 40, and 60 deg.

In Tunnel B heat-transfer rates were determined by the phase-change paint technique. The nominal test conditions were Mach 8 and free-stream Reynolds numbers based on model length (2 ft) of 5.0×10^6 and 7.4×10^6.

In Tunnel F heat-transfer rates were determined primarily by gage measurements with limited results obtained by the thermographic phosphor paint technique. A few pressure measurements were made in conjunction with the heat-transfer measurements. The nominal test conditions were Mach 10.5 and free-stream Reynolds numbers based on model length (2 ft) from 5.0×10^6 to 23.0×10^6.

In addition to the experimental program described above, a parallel analytic research program was conducted by the VKF under Air Force sponsorship. One particularly valuable result of this research was the development of a calculation technique for the laminar and turbulent windward surface heating of space shuttle configurations at large angles of attack. Results from the calculation are compared with the experimental results from the present program in this report, and a thorough description of the analytical procedures and additional data comparisons are presented in Ref. 19.

SECTION II
APPARATUS

2.1 WIND TUNNELS

2.1.1 Tunnel B

Tunnel B is a continuous, closed-circuit, variable density wind tunnel with an axisymmetric contoured nozzle and a 50-in.-diam test section. The tunnel can be operated at a nominal Mach number of 6 or 8 at stagnation pressures from 20 to 300 and 50 to 900 psia, respectively, at stagnation temperatures up to 1350°R. The model can be injected into the tunnel for a test run and then retracted for model cooling or model changes without interrupting the tunnel flow.

2.1.2 Tunnel F

Tunnel F is an electric-arc-heated impulse hypersonic wind tunnel of the hotshot type developed at AEDC. The test gas, nitrogen or air, is initially confined in an arc chamber by a diaphragm located near the throat of a convergent-divergent nozzle. The gas is heated and compressed by an electric arc discharge resulting in rupture of the diaphragm and subsequent expansion through a 4-deg half-angle conical nozzle to a maximum diameter of 108 in. Testing is possible at either the maximum diameter for Mach numbers from 13 to 22 or at the 54-in.-diam station for Mach numbers from 10 to 17. Useful run times between 50 and 200 msec are obtained. The present tests were conducted with nitrogen as the test gas at the 54-in.-diam station with a useful run time of approximately 100 msec utilizing the 4-cu-ft arc chamber.

2.2 MODELS

2.2.1 Tunnel B

Photographs and drawings of the models are presented in Figs. 1a and 2 (Appendix I), respectively. The original Tunnel B models were provided by the Langley Research Center and were fabricated with a 1/4-in. layer of Stycast® over a fiber-glass mandrel. The phase-change paint technique, which was used to provide heat-transfer-rate measurements in Tunnel B, requires a model material of relatively low thermal diffusivity to permit extraction of accurate heating data. Basically, the data are reduced by assuming

that the model wall temperature response is the same as a semi-infinite slab. Several materials have been used in wind tunnel tests which satisfy the semi-infinite slab requirement (within reasonable limits of time and material thickness). Probably the most commonly used material at present is Stycast, which is a filled, high-temperature epoxy. Stycast 2762 was selected as the model material for the present tests. However, during the June entry the Stycast cracked on the windward surface of the delta body and as a result the Stycast layer was removed and replaced with silcone rubber (RTV) prior to the September entry.

Chromel®-Alumel® thermocouples were cast into all the Stycast models approximately 1/8 in. from the surface to measure the initial model temperature.

2.2.2 Tunnel F

A photograph of the windward surface of the Langley delta wing model (LRC-DB) is shown in Fig. 1b. The LRC-DB and LRC-SB configurations (identification for this report) were instrumented identically along the windward centerline. A complete layout of the instrumentation and model details is shown in Fig. 2 for both Langley configurations. The models were designed and fabricated at Langley Research Center, Hampton, Virginia, from No. 416 stainless steel. A thin sheet metal cover was attached to the top surface to protect instrumentation leads and to streamline the flow in the sting region. The cover may be seen in the schlieren photographs presented in Fig. 3. The model dimensions corresponding to the instrumentation locations are tabulated in Ref. 16.

SECTION III
PROCEDURES

3.1 TEST CONDITIONS

A summary of the nominal test conditions is given in Table I (Appendix II). The specific test conditions with tabulated and graphical presentation of the data results are documented in two SADSAC reports (Refs. 15 and 16).

3.1.1 Tunnel B

The Tunnel B flow conditions are such that perfect gas, isentropic relationships can be used to compute test section properties. Flow calibrations are made periodically using a pitot tube rake, and these data are used to determine a mean test section Mach number. Using the calibrated Mach number and measured stilling chamber conditions (p_o and T_o), all test section properties can be computed.

3.1.2 Tunnel F

Since Tunnel F operates with a constant volume reservoir with an initial charge density, the reservoir conditions decay with time. As a result, all tunnel conditions and

model data results vary with time during the useful data range. Nondimensional values such as p_o'/p_o and model p/p_o' are relatively constant with time. Timewise variations in such parameters as Reynolds number permits acquisition of data at different Reynolds numbers for the same run. In many instances, laminar, transitional, and turbulent flow may be identified at the same gage location as a result of Reynolds number variation during one run. An illustration of the timewise behavior of various parameters for typical tunnel conditions encountered during this test is illustrated in Fig. 4.

To monitor the tunnel conditions, two 1.0-in.-diam hemisphere cylinders instrumented with slug-calorimeter-type heat-transfer gages were installed in the test section at an appropriate distance from the model to eliminate shock interference. A pitot probe was located near each hemisphere cylinder to measure the normal shock stagnation pressure. The reservoir pressure and pitot pressures were measured with strain-gage-type transducers.

The use of these measurements to compute flow conditions is summarized as follows: instantaneous values of p_o and p_o' and an instantaneous value of $\dot{q}_{ref}$ is inferred from the hemisphere-cylinder shoulder heat rate measurements. Stagnation enthalpy, H_o, is calculated from these measurements using Fay-Riddell theory (Ref. 20). With values of p_o, p_o', and H_o known, the remaining flow conditions (M_∞, Re_∞, etc.) are calculated as described in Refs. 21 and 22. For the short run times experienced in a hotshot tunnel, the model wall temperature ratio, T_w/T_t varies between 0.15 and 0.30 which approximates the range experienced with reentry vehicles. The flow conditions corresponding to results presented herein are provided in Table II along with the corresponding values of h_{ref}, and a Tunnel F test matrix is tabulated in Table III.

3.1.3 Test Condition Uncertainties

Uncertainty in the basic tunnel flow parameters p_o, T_o, p_o', and $\dot{q}_{ref}$ was estimated from repeat calibrations of the instrumentation and from repeatability and uniformity of the test section flows during tunnel calibrations. The individual contributions of these uncertainties were propagated through the appropriate flow equations to obtain the remaining uncertainties.

Approximate uncertainties in tunnel flow conditions are:

	Uncertainty, percent	
Parameter	Tunnel B	Tunnel F
p_o	±0.5	±5
p_o'	±0.3	±4
T_o	±1.0	±4
$\dot{q}_{ref}$	N/A	±5
M_∞	±0.3	±1.5

Parameter	Uncertainty, percent	
	Tunnel B	Tunnel F
p_∞	±2.0	±6
ρ_∞	±1.1	±8
U_∞	±0.5	±3
H_o	±1.4	±5
h_{ref}	±1.0	±2
$Re_{\infty,\ell}$	±2.0	±10

3.2 TEST PROCEDURES AND DATA REDUCTION

3.2.1 Phase-Change Paint Test Technique (Tunnel B)

The phase-change paint technique of obtaining heat-transfer data uses an opaque coating which changes phase from a solid to a liquid (melts) at a specific temperature. Tempilaq®, a paint consisting of calibrated melting point materials suspended in an inert carrier, was used as the phase-change indicator. The specific melting temperatures of the Tempilaq paints used were 113, 125, 163, 200, 250, 300, 350, and 400°F. Uncertainties in the phase-change temperatures are estimated by the manufacturer to be ±1 percent.

The primary data were obtained by photographing the progression of the melt lines with a 70-mm sequenced camera. The camera was mounted in the top window of the tunnel and photographed the model windward surface (model rolled 180 deg). The camera used TRI-X Pan Kodak® black-and-white film and the time from the start of model injection and of each shutter opening was recorded on magnetic tape. The camera was operated at two frames per second.

Backup data were obtained with a 16-mm motion-picture camera. This camera was operated at 24 frames per second, and Kodak Ektachrome EF® color film was used. The models were lighted with fluorescent light banks to minimize radiant heating of the models.

Prior to each run, the model was cleaned and cooled with alcohol and then spray-painted with Tempilaq. The model was installed on the model injection mechanism at the desired test attitude, and the model temperature was measured with a thermocouple probe or with the model-embedded thermocouples. During the course of the test, many of the embedded thermocouples became inoperative, and the probe temperature was generally used to determine the model initial temperature. The model was then injected into the airstream for approximately 15 sec, and during this time the model surface temperature rise produced isotherm melt lines.

The data reduction procedures used were somewhat more involved than previously used for paint data since the melt lines were transformed into body coordinates and the corresponding heat-transfer coefficients. The fundamentalsof this data reduction technique are described below.

During each run, the tunnel conditions and time of each picture were recorded on magnetic tape. The heat-transfer coefficient for each picture was calculated from the semi-infinite slab transient heat conduction equation.

$$\frac{T_{pc} - T_i}{T_{aw} - T_i} = 1 - e^{\beta^2} \operatorname{erfc} \beta$$

where $\beta = \frac{h\sqrt{\Delta t}}{\sqrt{\rho ck}}$, and $\sqrt{\rho ck} = 0.11\text{-}0.008\sqrt{\Delta t}$ for Stycast, and $\sqrt{\rho ck} = 0.037$ for RTV.

The equation for the thermal properties ($\sqrt{\rho ck}$) of Stycast was obtained by evaluation of a considerable amount of hemisphere calibration data and supplemented by VKF laboratory measurements. The value of $\sqrt{\rho ck}$ for RTV was obtained from Langley personnel.

Heat-transfer coefficients were calculated from assumed adiabatic wall temperatures of T_o, 0.9 T_o, and 0.85 T_o. The use of three values of T_{aw} provides an indication of the sensitivity of the heat-transfer coefficient (h) to the values of T_{aw} assumed (see Ref. 15). For the sake of consistency all plots and melt lines in this report are based on $T_{aw} = T_o$.

All heat-transfer coefficients were nondimensionalized by dividing by the stagnation point heat-transfer coefficient (Ref. 20) on a 0.675-in. radius sphere. The h_{ref} heat-transfer coefficients are tabulated in Table I.

The transformation of the melt line coordinates, as viewed by the camera (picture plane), to model coordinates is as follows. The 70-mm film was projected onto an 8- x 10-in. glass plate, and the melt contour coordinates were recorded on magnetic tape. In regions of relatively constant heating, a distinct melt line was frequently difficult to define, and in some cases the melt line tracings were terminated because of poor definition. A considerable amount of engineering judgement was involved in the interpretation of the melt patterns; consequently this was performed, or closely supervised, by an experienced engineer. To transform the melt lines into body coordinates the following additional steps were taken:

1. The model surface coordinates were measured at selected model stations with a modified Sheffield Cordax coordinate measuring machine (Model 200);

2. The camera location relative to the model was determined;

3. Using the principles of photogrammetry and the information obtained in steps 1 and 2, the model coordinates were transformed into the picture plane;

4. The body coordinates of a given melt line were then obtained by interpolation in the picture plane with the results being stored on magnetic tape.

The level of the heat-transfer coefficient associated with each melt line was obtained by the solution of the semi-infinite slab conduction equation as previously discussed. With the level and body coordinates of the heat-transfer coefficients stored on magnetic tape, any desired machine-generated plot within the limits of available data can be produced. Much of the phase-change paint data in this report are presented as data fairings obtained from machine-generated plots.

3.2.2 Gage Data (Tunnel F)

Model heat-transfer rates were measured with slug calorimeters and coaxial surface thermocouples. The slug calorimeters have a thin-film platinum resistance thermometer to sense the temperature of an aluminum disk which is exposed to the heat flux to be measured. The calorimeters are optimized to measure a given range of heat transfer by appropriate selection of the aluminum disk thickness. The coaxial surface thermocouple is comprised of an electrically insulated Chromel wire enclosed in a constantan cylindrical jacket. A thin film junction is made between the Chromel and constantan at the surface. In practical measurement applications, the surface thermocouple behaves as a homogeneous, one-dimensional, semi-infinite solid. The instrument provides an electromotive force (EMF) directly proportional to surface temperature which may be related by theory to the incident heat flux. All heat-transfer gages were bench calibrated prior to their installation into the model. The precision of these calibrations is estimated to be ±3 percent. Posttest calibrations were made for the majority of gages with calibration repeatability being within ±3 percent. A limited number of model pressure measurements were made by strain-gage-type transducers developed at the AEDC-VKF. Detailed information concerning all heat-transfer and pressure instrumentation and corresponding data reduction equations can be found in Ref. 23.

The accuracy of the data is a function not only of the uncertainty of the direct measurements but also of the test condition flow parameters. Assessments of the estimated uncertainties in individual data points based on instrument calibrations and run-to-run repeatability are as follows:

Parameter	Uncertainty, percent
p, psia	±5
$\dot{q}$, Btu/ft^2-sec	±9
h, Btu/ft^2-sec-°R*	±10

*The uncertainty in h was determined by the same method as h_{ref} (see Section 3.1.2).

3.2.3 Phosphor Paint Technique (Tunnel F)

Because of certain unique problems particular to high angle-of-attack testing on the windward surface such as the paint application procedure and shock glow, a limited amount of phosphor paint results were obtained on the Langley configurations. A brief description of the phosphor paint technique is reported herein. The reader should refer to Ref. 18 for a complete description of the phosphor paint technique as used in Tunnel F.

The phosphorescent paint technique consists of photographing the painted model surface and measuring the optical density of the recorded image. An ultraviolet light is used to excite the phosphorescence of the paint. Two view-cameras located at an optical port on the bottom of the tunnel with 163-mm lens and 4- x 5-in. Polaroid® backs were used to record the pictures on Type 57 Polaroid (ASA 3000) film. Each camera had a set of filters to pass only the 5000- to 6000-Å light emitted by the paint. The optical density distributions of the pictures were read and recorded on magnetic tape by a P-1000 Photoscan® microdensitometer manufactured by Optronics International. The data on the magnetic tapes were input to the VKF digital computer which was used to create contour mappings of the optical density. The optical density is related to heat-transfer rate by measuring a few heat-transfer rates with standard heat-transfer instrumentation at the same time the paint pictures are taken. Heat-transfer rates as determined from gages give a calibration for the paint, since it can be shown that the optical density is proportional to the model heat-transfer rate. Therefore, by relating the paint data to the heat gage measurements, the paint data yield the detailed heat-transfer-rate distribution over the model.

A sample of a reduced phosphor paint picture on the LRC-SB configuration is shown in Fig. 5. The model image is distorted by the viewing angle of the camera and, consequently, is reflected in the final contour mapping. Automated procedures are available whereby one may obtain body coordinates directly from the picture plane coordinates as described in Section 3.2.1.

SECTION IV
RESULTS AND DISCUSSION

This section documents results pertaining to the windward shock angles and pressure distributions at Mach ≈10.5 and windward centerline and spanwise heat-transfer distributions at Mach 8 and 10.5. Comparisons are made between experiment and theory where appropriate. A detailed description of the theoretical applications presented herein may be found in Ref. 19.

4.1 SHOCK ANGLE AND SURFACE PRESSURE

Experimental shock angle measurements and limited centerline pressure distributions are presented in Figs. 6 and 7, respectively, at Mach number 10.5 for angles of attack of 20, 40, and 60 deg for the LRC-DB and LRC-SB configurations. The shock angle results

shown in Fig. 6 are presented in terms of the incremental angle between the local body slope and the local bow shock. The incremental angles are compared with a conical shock and an empirical fit from Ref. 24. Although the empirical fit of Ref. 24 (Eq. 10)) is from sharp-leading-edge delta wing numerical solutions, the results are in good agreement with this experiment. At α = 20 and 40 deg, the conical shock theory is within 1 deg of the data on the LRC-DB configuration. However, the change in body shape (at x/ℓ = 0.33) of the LRC-SB configuration obviously changed the bow shock angle at α = 40 and 60 deg. The different shock shapes are further illustrated with the schlieren photographs shown in Fig. 3 at a 40-deg angle of attack.

Limited pressure distributions are presented in Fig. 7 for both configurations at Mach number 10.5 for angles of attack of 20, 40, and 60 deg. The experimental results are bracketed by simple theories at 20- and 40-deg angle of attack, and the modified Newtonian theory is in reasonable agreement with the pressure measurements on the aft section of the model at a 60-deg angle of attack. There is a considerable pressure decay for the LRC-SB configuration at 40- and 60-deg angles of attack. A 20-deg half-angle sphere cone characteristics solution at zero angle of attack is also compared to data at a 20-deg angle of attack. This solution is in good agreement with the experiment and is included since it was used in making some of the theoretical heat-transfer calculations. To add validity to the above procedure, pressure data results from Langley Research Center at Mach 8 and 20-deg angle of attack on the LRC-DB configuration (Ref. 25) were analyzed and found to be in good agreement over the complete windward centerline with a characteristic solution for a 20-deg half-angle sphere cone.

4.2 HEATING DISTRIBUTIONS

The results of the heat-transfer measurements are shown in Figs. 8 through 13. Heat-transfer coefficients presented at Mach number 8 were obtained using the phase-change paint technique. Typical photographs using the phase-change paint are presented in Fig. 8. Isotherm lines are indicated by the dark model surface showing through the white paint (Tempilaq). The Mach number 10.5 heat-transfer coefficients were obtained using heat-transfer sensors.

The windward centerline heating distributions at α = 20, 40, and 60 deg for Mach numbers 8 and 10.5 are presented in Figs. 9 and 10, respectively. The 20-deg angle-of-attack data are compared with two-dimensional laminar and turbulent numerical boundary-layer solutions without crossflow. The edge conditions were calculated using experimental shock (shock angle = 23.5 deg) and normal shock conditions. The input pressure distribution was for a 20-deg half-angle sphere cone at zero-degree angle of attack as illustrated in Fig. 7. A more complete discussion of the two-dimensional boundary-layer equations with comparisons and applications are illustrated in Ref. 17.

The laminar and turbulent theoretical distributions at α = 40 and 60 deg were calculated by the method described in Ref. 19. Inviscid conical flow was assumed for the 40-deg angle-of-attack calculations while a shock angle equal to the body angle and

equal to the experimental shock angle were both considered at α = 60 deg. The crossflow inviscid velocity gradient was obtained by approximating the local body lower surface with a rounded-shoulder flat-face cylinder using the one-strip method of integral relations from South (Ref. 26). Additional data comparisons and a more complete description of the theoretical calculations used herein are presented in Ref. 19.

Mach 8 heat-transfer distributions along the windward centerline obtained using the phase change paint technique at α = 20, 40, and 60 deg are presented in Fig. 9. At α = 20 deg the laminar data are above the theory, but it should be pointed out that for $x/\ell \leq 0.1$ the gradient is so steep that a relatively small error in the x/ℓ values could account for some of this discrepancy. For $x/\ell \approx 0.5$ the data are transitional and appear to be approaching the turbulent level based on edge conditions obtained from the experimental shock angle. The α = 40 deg LRC-DB data show excellent agreement with both the laminar and turbulent levels predicted by crossflow theory (Ref. 19). However, the LRC-SB data overshoot the turbulent theory, and to date the cause of this discrepancy is unknown. The α = 60-deg data indicate transitional conditions occur at about x/ℓ = 0.4, and upstream of this point there is good agreement with theory.

In Fig. 10, Mach 10.5 heat-transfer-rate gage data for both configurations at 20-, 40-, and 60-deg angles of attack are compared to theoretical solutions calculated in the same manner as previously discussed. Based on a thorough analysis of these results and the Mach 10.5 results reported in Ref. 18, it was concluded that the majority of the Tunnel F results were influenced by surface roughness such as pressure orifices and heat gages that unintentionally "tripped" the boundary layer at high angle of attack. Transition onset was definitely traced to pressure orifices by optical data, and these results are reported in Ref. 18. With special precautions in model preparation and gage installation, some "natural" transitional results were obtained on the McDonnell-Douglas orbiter model at α = 40 deg. A complete discussion and analysis of the orbiter model Tunnel F transition results is presented in Ref. 18.

The experimental results at $Re_{\infty,\ell} \approx 10 \times 10^6$ at Mach 10.5 include two or three runs as illustrated by the large number of symbols in Fig. 10. The α = 20-deg results on the aft section of the model are in good agreement with the two-dimensional turbulent calculation based on experimental shock edge conditions. There is no discernible difference in level between the two configurations. The results at α = 40 deg are in good agreement with the turbulent crossflow theory (Ref. 19) based on conical shock conditions. There is a tendency for the LRC-SB configuration heat-transfer results to have a higher level than the LRC-DB results. The results at a 60-deg angle of attack are compared with turbulent crossflow theory (Ref. 19) using a shock angle equal to 60 deg (parallel shock) and an experimental shock distribution. As noted in Fig. 6 there is a considerable difference in the shock angle between the two configurations. Since the Newtonian pressure used to make the theoretical calculations was in reasonable agreement with experiment, the pressure values were not adjusted. Both configurations are in excellent agreement with the theoretical calculation based on the experimental shock.

The effect of Reynolds number on the LRC-DB heating distributions at a 40-deg angle of attack for Mach 8 and 10.5 is presented in Fig. 11. The limited turbulent data at Mach 8 are in good agreement with theory. As expected, the high Reynolds number condition ($Re_{\infty,\ell} = 7.4 \times 10^6$) caused transition on the model surface to move upstream. The Mach 10.5 results illustrate the theoretical turbulent Reynolds number scaling over a large Reynolds number range. The experimental results are in good agreement with theory at all three Reynolds numbers. The Mach number 10.5 results illustrate the inability of the parameter h/h_{ref} to collapse turbulent heating data at different Reynolds numbers to a single curve. This can be attributed to the use of h_{ref} which is based on laminar considerations and varies as the $\sqrt{Re_{\infty,\ell}}$, whereas the measured turbulent heating rates vary as the $\sqrt[5]{Re_{\infty,\ell}}$. Consequently, the scaling of the turbulent heat-transfer coefficient (h) nondimensionalized by h_{ref} should scale as follows:

$$h/h_{ref} \propto (Re_{\infty,\ell} \text{ Ratio})^{0.3}$$

Comparison of experimental and theoretical spanwise heating distributions at Mach numbers 8 and 10.5 are presented in Figs. 12 and 13 for both configurations. The theoretical calculations were obtained by assuming inviscid conical flow along the centerline for α = 40 deg and an experimental shock for α = 60 deg. The spanwise surface pressure distribution was obtained by approximating the local body lower surface with a rounded-shoulder flat-face cylinder using the one-strip method of integral relations from South (Ref. 26). A complete description of the calculation procedures for the theoretical spanwise distributions is presented in Ref. 19.

The Mach 8 spanwise heat-transfer distributions (Fig. 12) are shown at $x/\ell = 0.3$ and 0.7 for α = 20, 40, and 60 deg. In general, these distributions are as expected with the exception of the α = 40 data at $x/\ell = 0.3$ and the α = 20 data at $x/\ell = 0.7$. The cause of the variations in these data could be attributed to crossflow transition, nose bluntness effects, relaminarization, or a combination of these.

Comparison of experimental and theoretical spanwise pressure and heat-transfer distributions at Mach 10.5 and $x/\ell = 0.743$ are shown in Fig. 13. The theoretical solutions were calculated as discussed above Reference theoretical calculations at $y/y_{max} = 0$ are noted at α = 20 deg, and the theoretical calculations are in reasonable agreement with the experimental results at α = 40 and 60 deg. The spanwise pressure decay with distance (y/y_{max}) is more severe for the LRC-SB configuration at all angles of attack. In general, the $M_\infty \approx 10.5$ LRC-DB experimental heat-transfer results are higher than the LRC-SB results contrary to the theoretical results. It is interesting to note that both the M_∞ = 8.0 and 10.5 spanwise data exhibit characteristics which are not easy to explain even though the configurations are relatively simple shapes.

4.3 BOUNDARY-LAYER TRANSITION

Heat-transfer measurements as documented in Figs. 9, 10, and 11 were used to evaluate the onset of transition. As previously mentioned, it was concluded that the Tunnel F

results were influenced by surface roughness such as pressure orifices and heat gages that unintentionally "tripped" the boundary layer. A complete discussion of surface roughness effects and general procedures for analyzing transition data results are presented in Ref. 18. Transition Reynolds number data from the AEDC-VKF Tunnels B and F are presented in Fig. 14 in terms of the Kipp-Masek (Ref. 28) correlating parameters. A similar plot is presented in Ref. 18 with the McDonnell-Douglas delta wing orbiter results including a description of the method of calculating the correlating parameters. The following observations are made from Fig. 14:

1. The revised best fit of the correlated data was determined from delta wing data having a large scatter band.

2. The Tunnel B transition data are in good agreement with the revised best-fit fairing.

3. Agreement or disagreement of experimental transition results with the best-fit correlating curve should not be the sole factor used to establish whether transition data are "good" or "bad". Data affected by surface roughness can lie within the correlating data scatter band as illustrated by the Tunnel F tripped data.

SECTION V
CONCLUSIONS

Based on the results presented herein, the conclusions are:

1. The geometry change on the LRC-SB configurations at $x/\ell \approx 0.33$ changes the shock shape which in turn promotes a pressure decay on the model centerline windward ray for $x/\ell \geq 0.4$ for α = 40 and 60 deg.

2. In most cases the centerline heating distributions at Mach 8 and 10.5 are in good agreement with the applicable theory.

3. The spanwise heating distributions at Mach 8 and 10.5 are in general agreement with most theoretical comparisons; however, some of the data trends cannot be explained theoretically.

4. Agreement or disagreement of experimental transition results with the best-fit correlating curve of Kipp and Masek should not be the sole factor used to establish whether transition data are "good" or "bad". Data affected by surface roughness can lie within the correlating data scatter band.

REFERENCES

1. Matthews, R. K., Martindale, W. R., and Warmbrod, J. D. "Heat Transfer Tests of the McDonnell-Douglas Delta Wing Orbiter Mated with -17A Booster at Mach Number 8." NASA CR-120,067, May 1972.

2. Matthews, R. K., Martindale, W. R., and Warmbrod, J. D. "Heat Transfer Test of the McDonnell-Douglas Delta Wing Orbiter and the -17A Booster (not Mated) at Mach Number 8." NASA CR-120,068, May 1972.

3. Matthews, R. K., Martindale, W. R., and Warmbrod, J. D. "Heat Transfer Rate Distributions on McDonnell-Douglas Booster Determined by Phase Change Technique for Nominal Mach Number of 8." NASA CR-120,043, April 1972.

4. Matthews, R. K., Martindale, W. R., and Warmbrod, J. D. "Surface Pressure and Inviscid Flow Field Properties McDonnell-Douglas Booster Nominal Mach Number of 8." NASA CR-120,047, March 1972.

5. Martindale, W. R., Matthews, R. K., and Warmbrod, J. D. "Heat Transfer Rate Distributions on the McDonnell-Douglas Delta Wing Orbiter at a Mach Number of 8." NASA CR-120,025, June 1972.

6. Warmbrod, J. D., Martindale, W. R., and Matthews, R. K. "Surface Pressure and Inviscid Flow Field Properties of the McDonnell-Douglas Delta-Wing Orbiter for Nominal Mach Number of 8." NASA CR-120,037, January 1972.

7. Eaves, R. H., Buchanan, T. D., and Warmbrod, J. D. "Heat Transfer Investigation of the McDonnell-Douglas Delta Wing Orbiter at a Nominal Mach Number of 10.5." NASA CR-120,024, May 1972.

8. Warmbrod, J. D., Martindale, W. R., and Matthews, R. K. "Heat Transfer Rate Measurements on Convair Booster (B-15B-2) and North American Rockwell Orbiter (161B) at Nominal Mach Number of 8." NASA CR-120, 009, November 1971.

9. Warmbrod, J. D., Martindale, W. R., and Matthews, R. K. "Heat Transfer Rate Measurements on Convair Booster (B-15B-2) at Nominal Mach Number of 8." NASA CR-119, 987, November 1971.

10. Warmbrod, J. D., Martindale, W. R., and Matthews, R. K. "Heat Transfer Rate Measurements on North American Rockwell Orbiter (161B) at Nominal Mach Number of 8." NASA CR-120, 029, December 1971.

11. Matthews, R. K., Martindale, W. R., and Warmbrod, J. D. "Heat Transfer Rate Distribution on North American Rockwell Delta Wing Orbiter Determined by Phase Change Paint Technique at a Mach Number of 8." NASA CR-120,048, March 1972.

12. Matthews, R. K., Martindale, W. R., and Warmbrod, J. D. "Surface Pressure and Inviscid Flow Field Properties of the North American Rockwell Delta-Wing Orbiter for Nominal Mach Number of 8." NASA CR-120,046, March 1972.

13. Matthews, R. K., Martindale, W. R., and Warmbrod, J. D. "Ascent Heat Transfer Rate Distributions on Tests of the NR Delta Wing Orbiter and GD/C Booster at Mach Number 8 (Mated)." NASA CR-120,049, July 1972.

14. Matthews, R. K., Martindale, W. R., and Warmbrod, J. D. "Ascent Heat Transfer Rate Distributions on the NR Delta Wing Orbiter and the GD/C Booster at Mach Number 8 (not Mated)." NASA CR-120,071, July 1972.

15. Matthews, R. K., Martindale, W. R., Warmbrod, J. D., and Johnson, C. B. "Heat Transfer Investigation of Langley Research Center Transition Models at a Mach Number of 8." NASA CR-120,045, March 1972.

16. Eaves, R. H., Buchanan, T. D., Warmbrod, J. D., and Johnson, C. B. "Heat Transfer Investigation of Two Langley Research Center Delta Wing Configurations at a Mach Number of 10.5." NASA CR-120,036, March 1972.

17. Martindale, W. R., Matthews, R. K., and Trimmer, L. L. "Heat Transfer and Flow Field Tests of the North American Rockwell/General Dynamics Space Shuttle Configurations." AEDC-TR-72-169, January 1973.

18. Matthews, R. K., Eaves, R. H., Jr., and Martindale, W. R. "Heat Transfer and Flow Field Tests of the McDonnell Douglas-Martin Marietta Space Shuttle Configurations." AEDC-TR-, to be published.

19. Adams, J. C., Jr. and Martindale, W. R. "Hypersonic Lifting Body Windward Surface Flow Field Analysis for High Angles of Incidence." AEDC-TR-73-2, to be published.

20. Fay, J. A. and Riddell, F. R. "Theory of Stagnation Point Heat Transfer in Dissociated Air." Journal of Aerospace Sciences, Vol. 25, No. 2, pp. 73-85, 121, February 1958.

21. Grabau, Martin, Smithson, H. K., Jr., and Little, Wanda J. "A Data Reduction Program for Hotshot Tunnels Based on the Fay-Riddell Heat-Transfer-Rate Using Nitrogen at Stagnation Temperatures from 1500 to 5000°K." AEDC-TR-64-50 (AD601070), June 1964.

22. Griffith, B. J. and Lewis. C. H. "A Study of Laminar Heat Transfer to Spherically Blunted Cones at Hypersonic Conditions." AEDC-TDR-63-102 (AD408568), June 1963. Also AIAA Journal, Vol. 2, No. 3, pp. 438-444, March 1964.

23. Ledford, R. L., Smotherman, W. E., and Kidd, C. T. "Recent Developments in Heat-Transfer Rate, Pressure, and Force Measurements for Hotshot Tunnels." AEDC-TR-66-228 (AD645764), January 1967.

24. Nagel, A. L., Fitzsimmons, H. D., Doyle, L. B. "Analysis of Hypersonic Pressure and Heat-Transfer Tests on Delta Wings with Laminar and Turbulent Boundary Layers." NASA CR-535, August 1966.

25. Lordi, J. A., Vidal, R. J., Johnson, C. B. "Chemical Nonequilibrium Effects on the Flow in the Windward Plane of Symmetry of a Blunted Delta Orbiter." NASA TM X-2506, Vol. I, page 185, February 1972.

26. South, J. C., Jr. "Calculations of Axisymmetric Supersonic Flow Past Blunt Bodies with Sonic Corners Including a Program Description and Listing." NASA TN D-4563, May 1968.

27. Kipp, H. W. and Masek, R. V. "Aerodynamic Heating Constraints on Space Shuttle Vehicle Design." ASME Paper 70-HI/SPI-45, June 1970.

28. Fehrman, A. L. and Masek, R. V. "Study of Uncertainties of Predicting Space Shuttle Thermal Environment." MDC E0639, June 1972.

APPENDIXES

I. ILLUSTRATIONS

II. TABLES

Preceding page blank

a. Straight Body (LRC-SB), Tunnel B

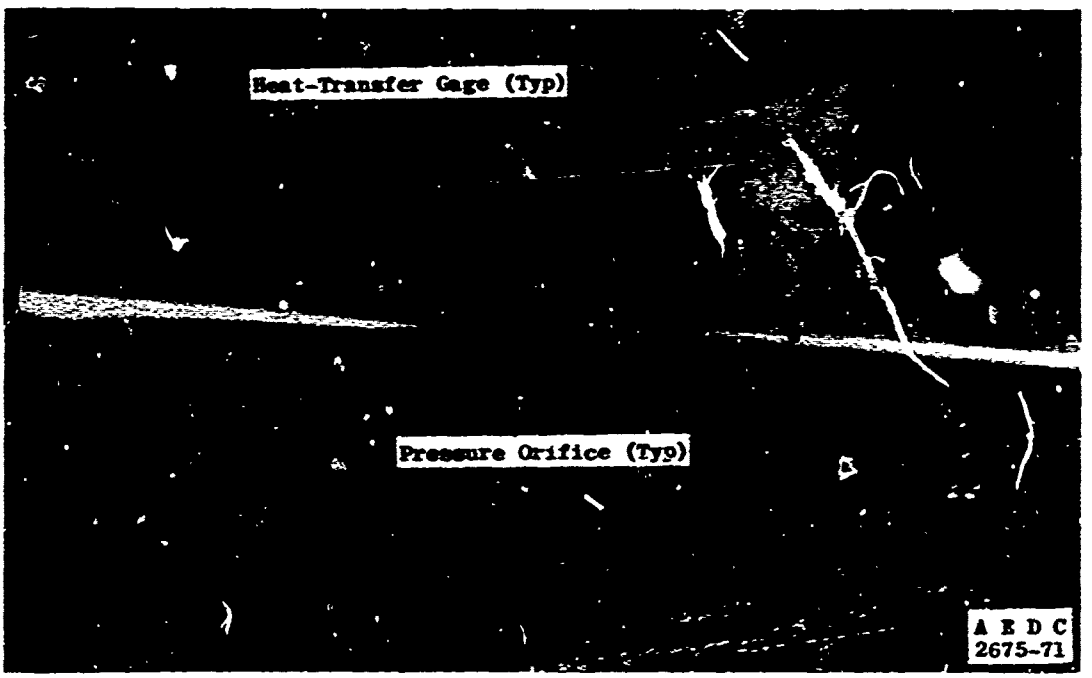

b. Delta Body (LRC-DB), Tunnel F

Fig. 1 Model Photographs

Preceding page blank

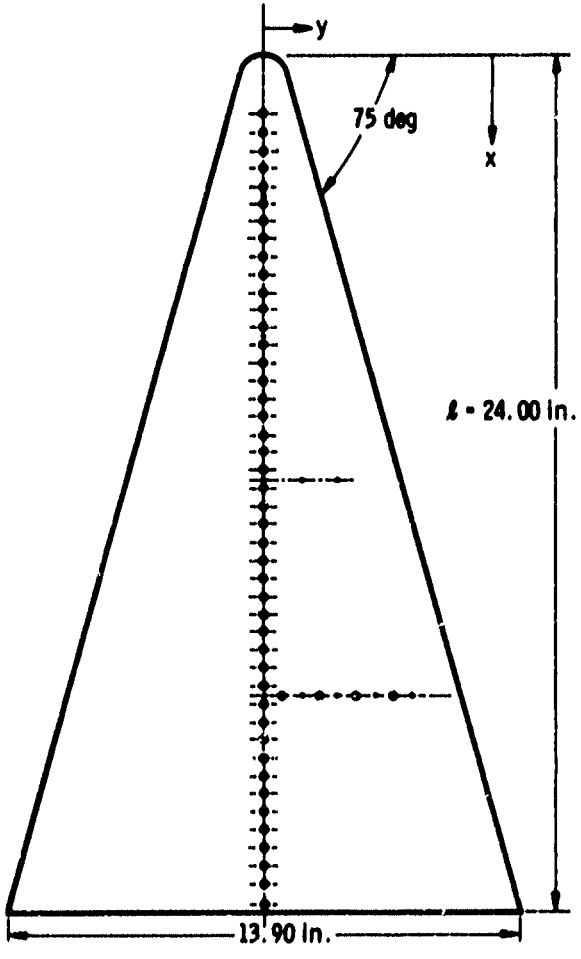

a. LRC-DB Model

Side View

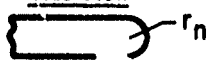

r_n (Profile Radius) ~ 0.675 in.

Cross-Section

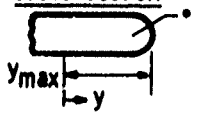

* 0.675-in. Radius Cut Normal to Leading Edge

Tunnel F Instrumentation

- • Pressure Orifice
- ○ Heat-Transfer Sensor

Notes:
1. The model dimensions for the Tunnel B and F models are the same.
2. Instrumentation details are shown for Tunnel F models. There was no instrumentation on the Tunnel B models.
3. The leeward surface was streamlined for sting attachment. Complete details of the leeward surface geometry is reported in Refs. 15 and 16.

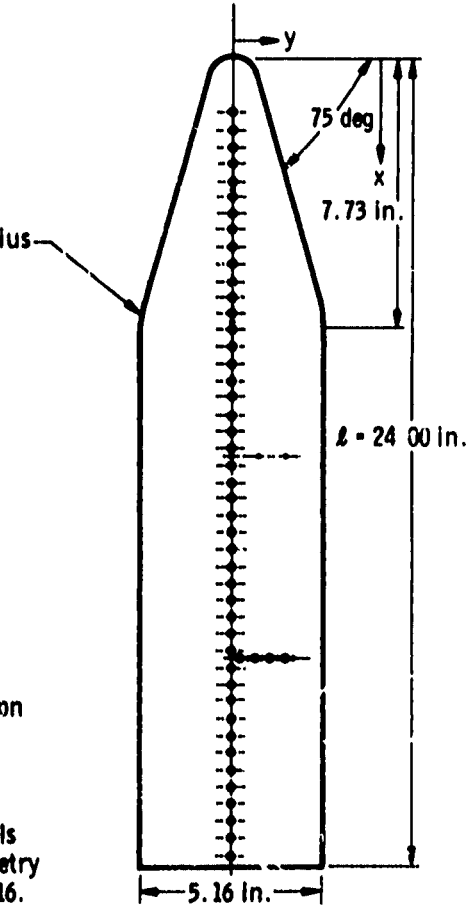

b. LRC-SB Model

Fig. 2 Model Sketches

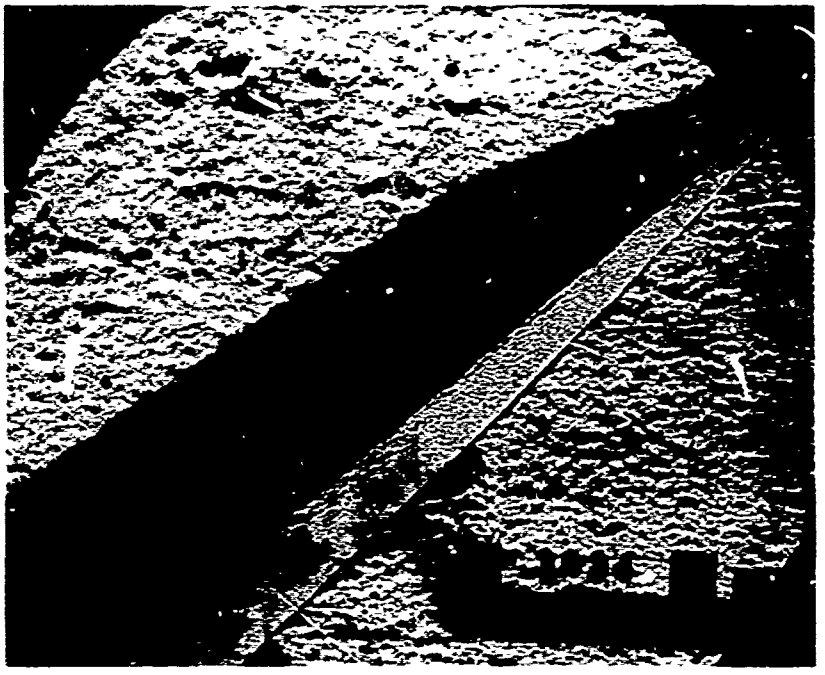

a. LRC-DB, $Re_{\infty,\ell} = 9.8 \times 10^6$

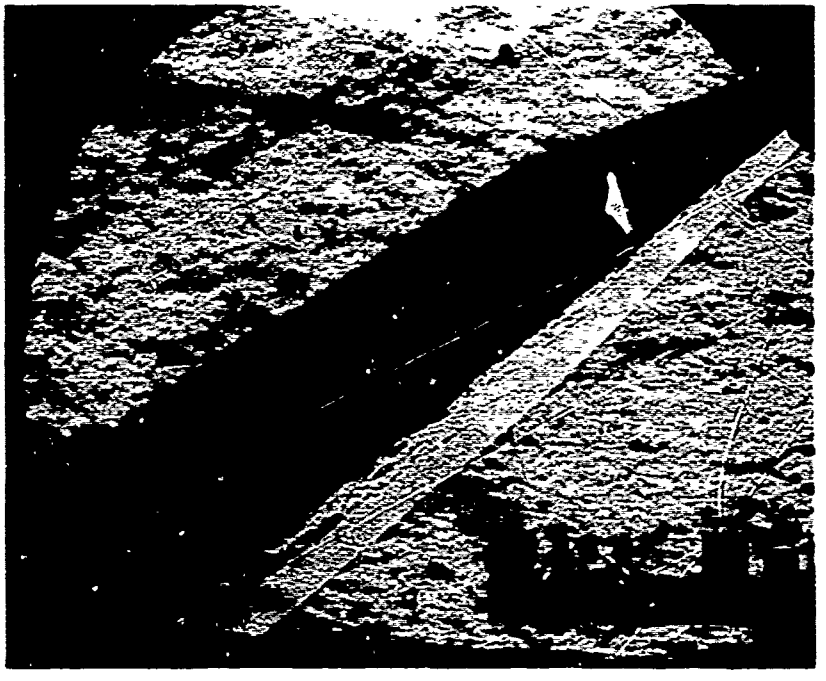

b. LRC-SB, $Re_{\infty,\ell} = 15.3 \times 10^6$

Fig. 3 Schlieren Photographs at 40-deg Angle of Attack, $M_\infty \approx 10.5$

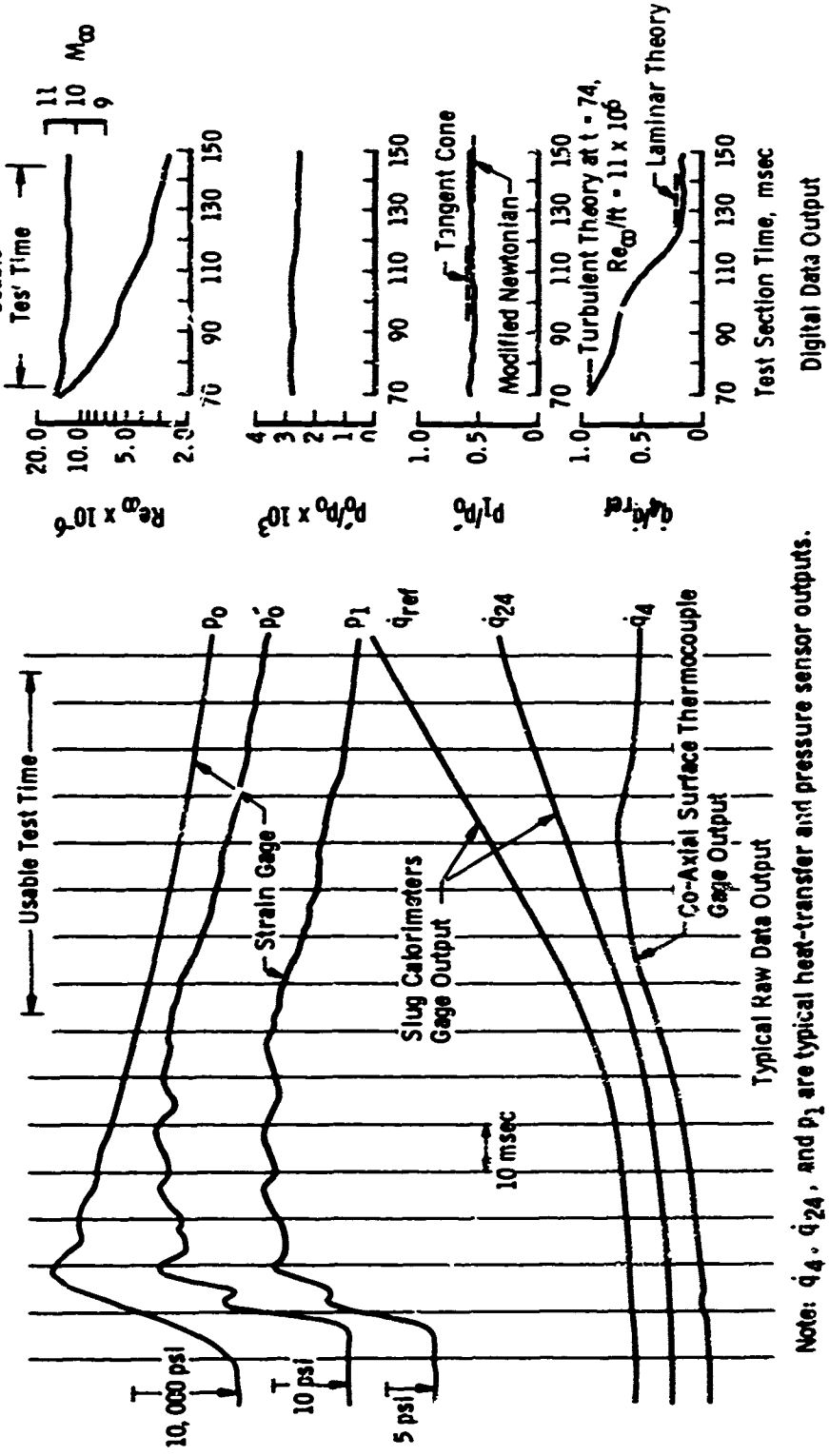

Note: $\dot{q}_4$, $\dot{q}_{24}$, and p_1 are typical heat-transfer and pressure sensor outputs.

Fig. 4 Typical Timewise Variation of Tunnel Conditions and Model Data at $M_\infty \approx 10.5$ (Tunnel F)

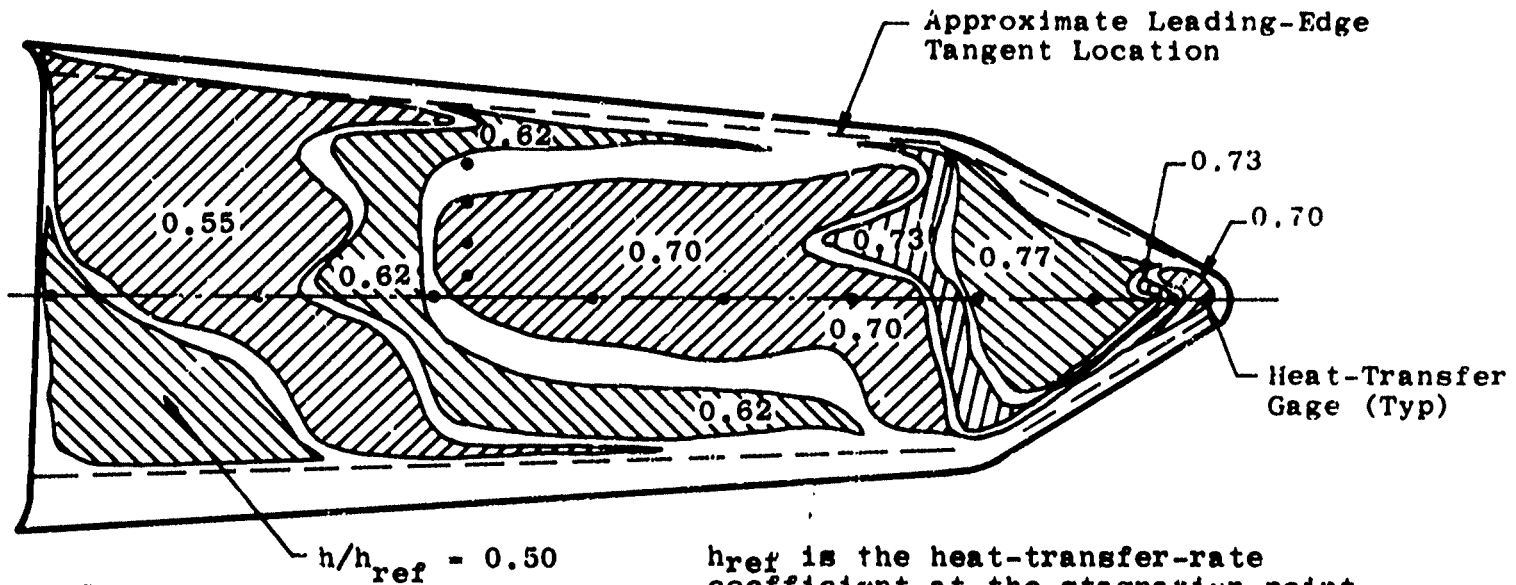

Run 3645
α = 40 deg
M_∞ = 10.6
$Re_{\infty,\ell}$ = 12.8 x 10^6
h_{ref} = 0.0495 Btu/ft^2-sec-^oR

h_{ref} is the heat-transfer-rate coefficient at the stagnation point of a 1-in. diam hemisphere-cylinder probe adjusted to a 0.675-in. nose radius.

Fig. 5 Sample of Thermographic Phosphor Paint Results at $M_\infty \approx 10.5$ (Tunnel F)

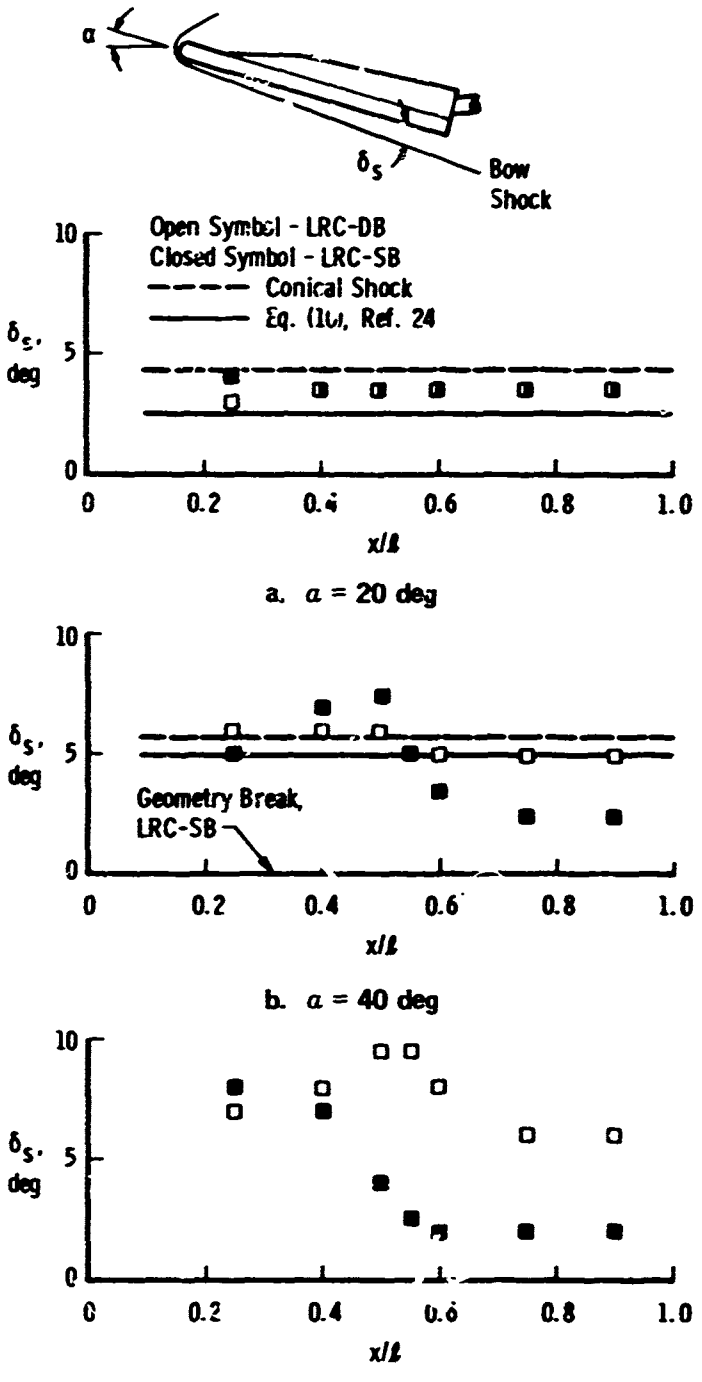

Fig. 6 Comparison of Experimental and Theoretical Shock Angles at $M_\infty \approx 10.5$ (Tunnel F)

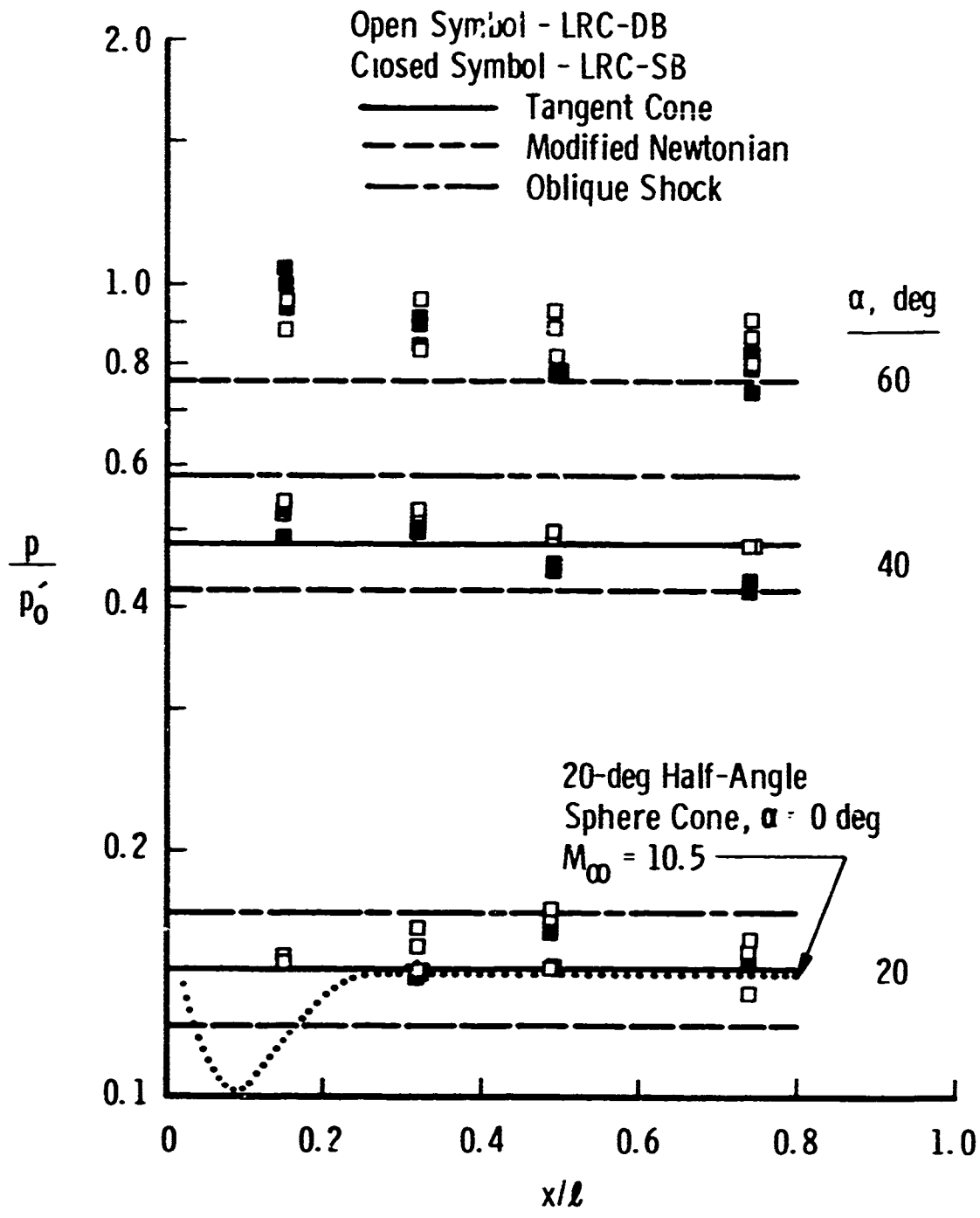

Fig. 7 Comparison of Experimental and Theoretical Windward Centerline Pressure Distributions at $M_\infty \approx 10.5$ and $Re_{\infty,\ell} \approx 10 \times 10^6$ (Tunnel F)

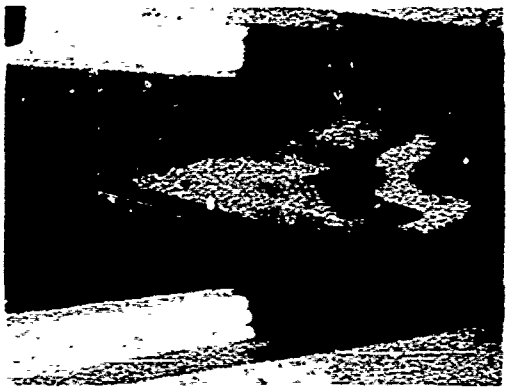

a. α = 20 deg

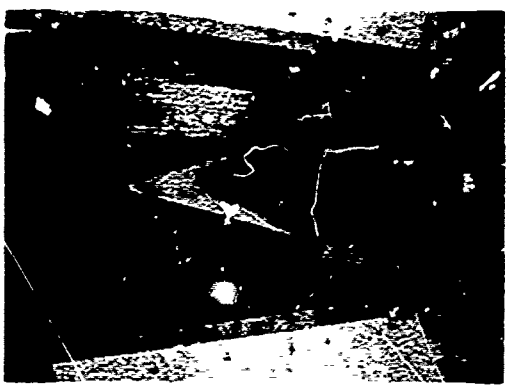

b. α = 40 deg

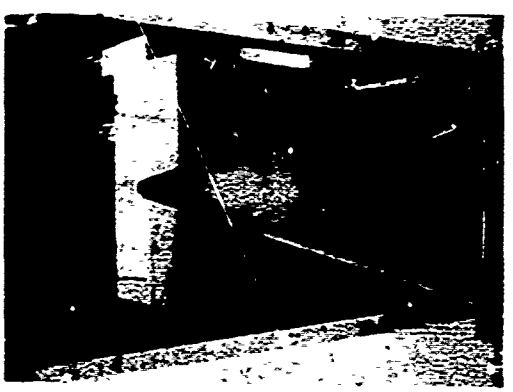

c. α = 60 deg

Fig. 8 Typical Phase-Change Photographs at M_∞ = 8 and $Re_{\infty,\ell}$ = 7.4 x 10^6 (Tunnel B)

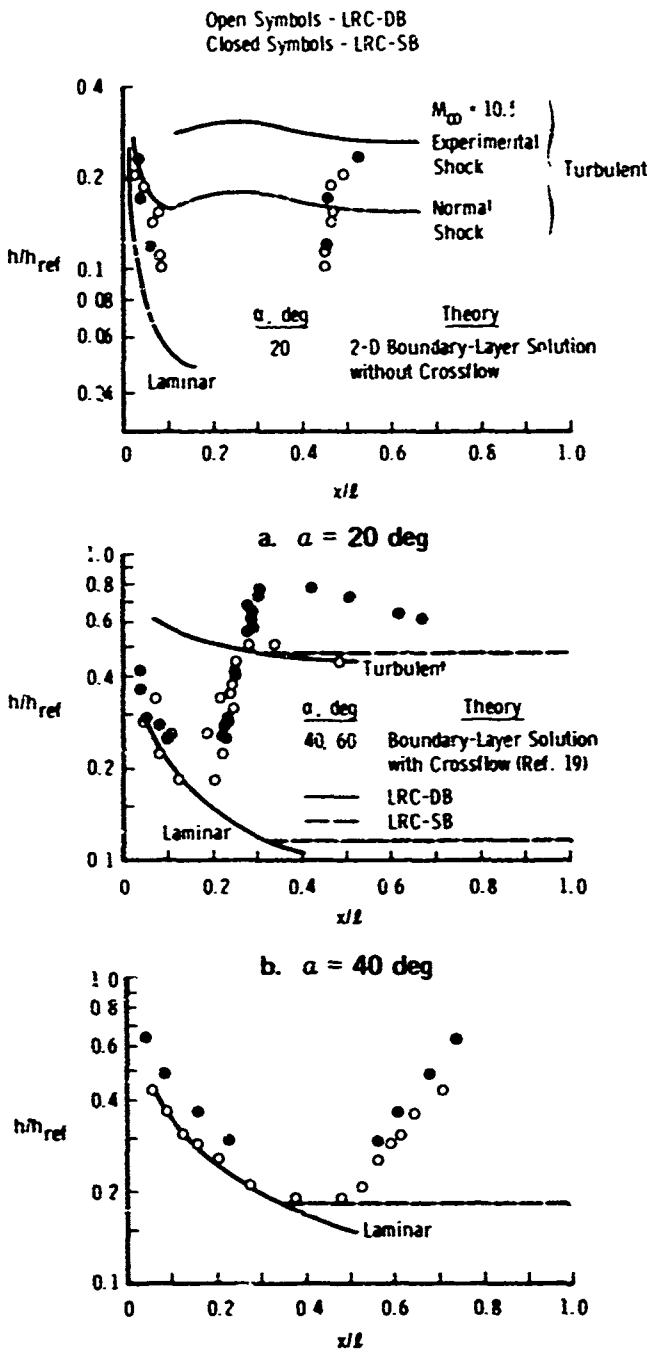

Fig. 9 Comparison of Experimental and Theoretical Windward Centerline Heating Distributions at M_∞ = 8 and $Re_\infty \ell = 7.4 \times 10^6$ (Tunnel B)

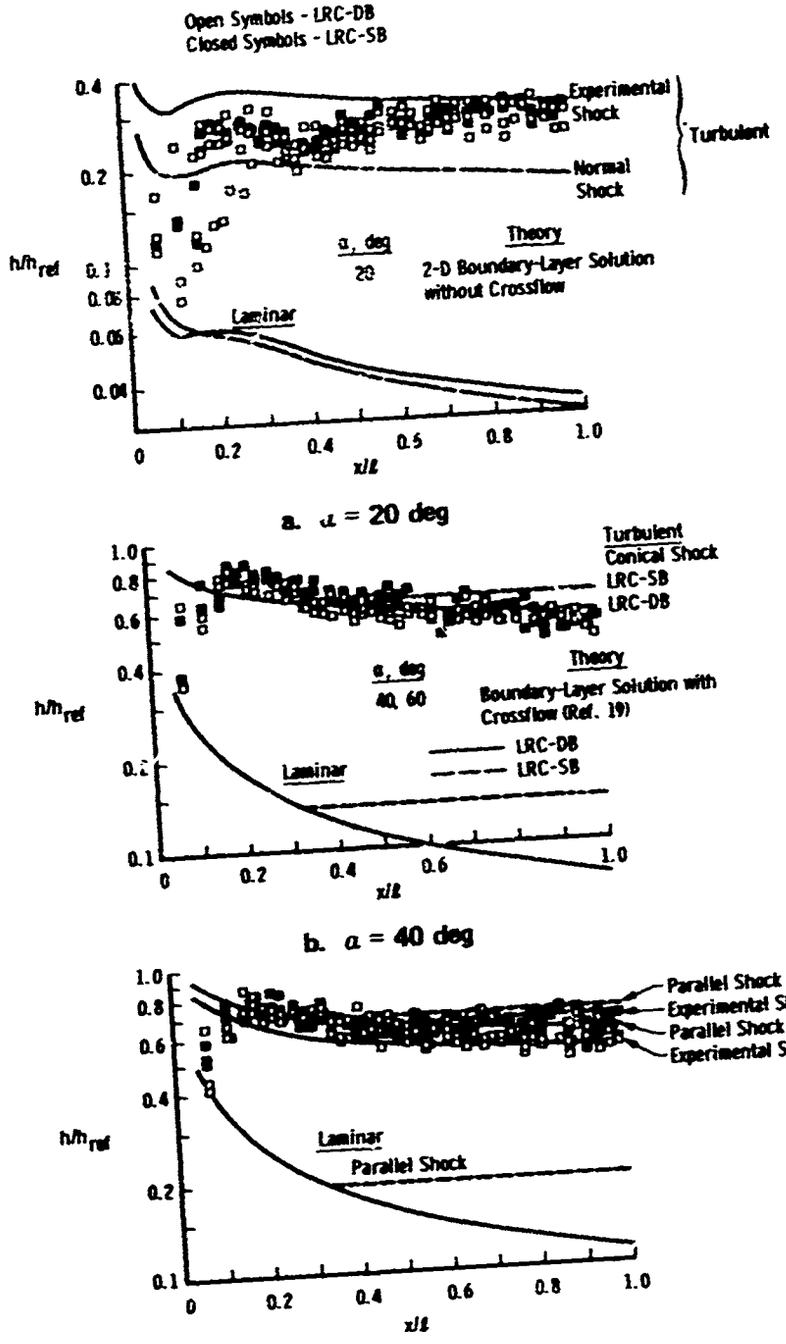

Fig. 10 Comparison of Experimental and Theoretical Windward Centerline Heating Distributions at $M_\infty \approx 10.5$ and $Re_{\infty,\ell} = 10 \times 10^6$ (Tunnel F)

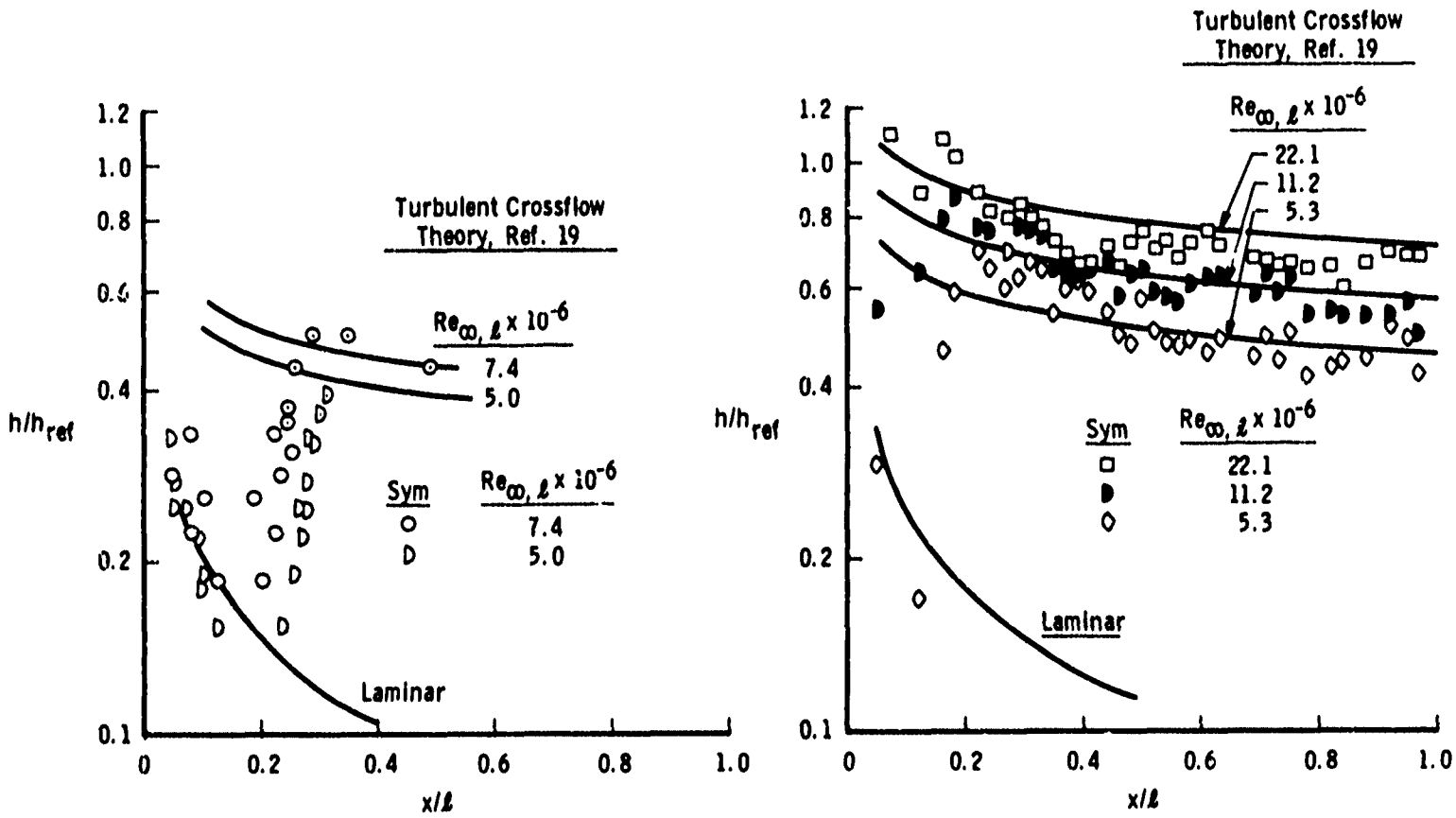

a. $M_\infty = 8$ (Tunnel B)

b. $M_\infty \approx 10.5$ (Tunnel F)

Fig. 11 Effect of Reynolds Number on Normalized Heat-Transfer Heating Distributions on the LRC-DB Configuration at 40-deg Angle of Attack

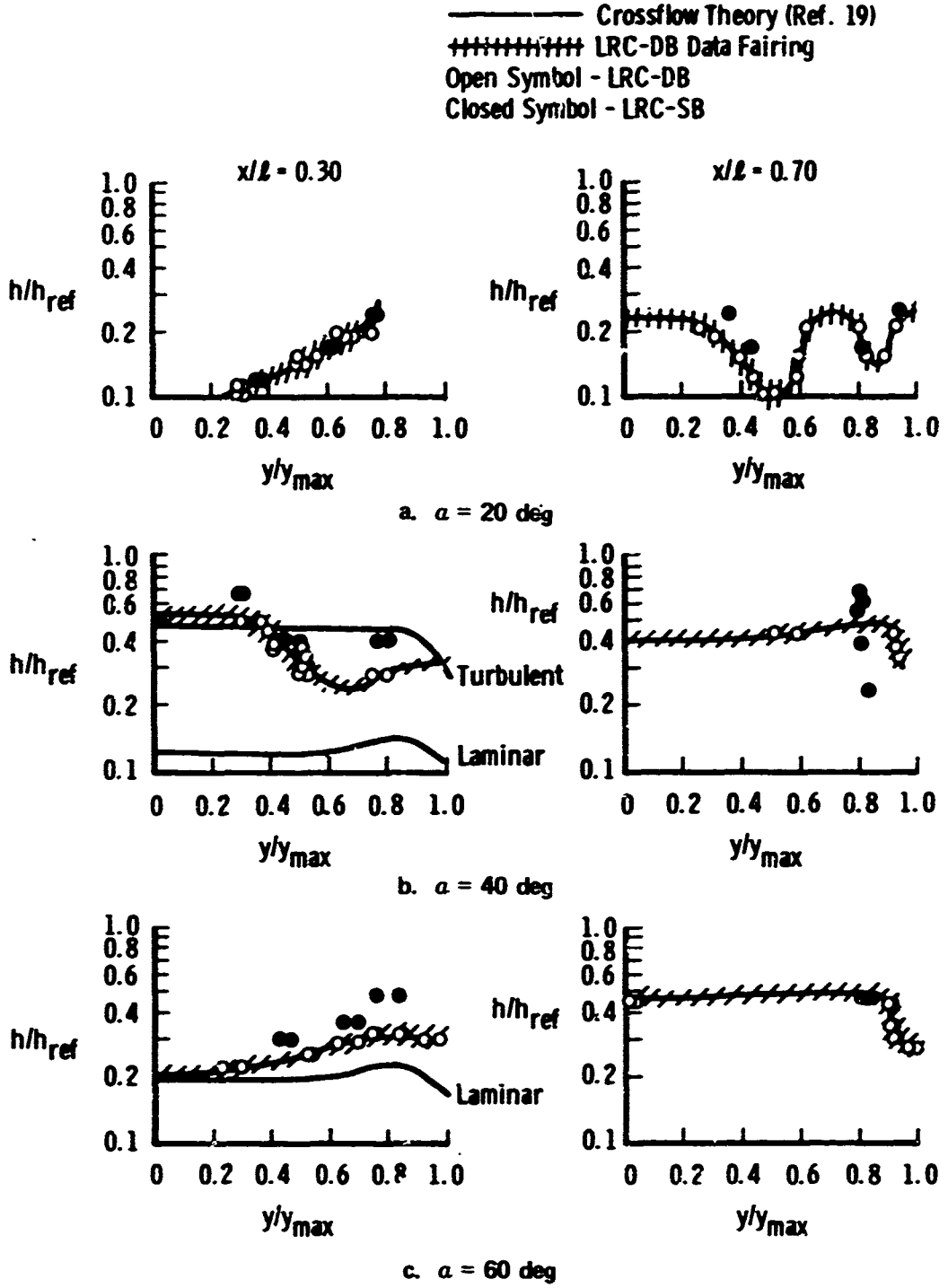

Fig. 12 Comparison of Experimental and Theoretical Spanwise Heating Distributions at $M_\infty = 8$ and $Re_{\infty,\ell} = 7.4 \times 10^6$ (Tunnel B)

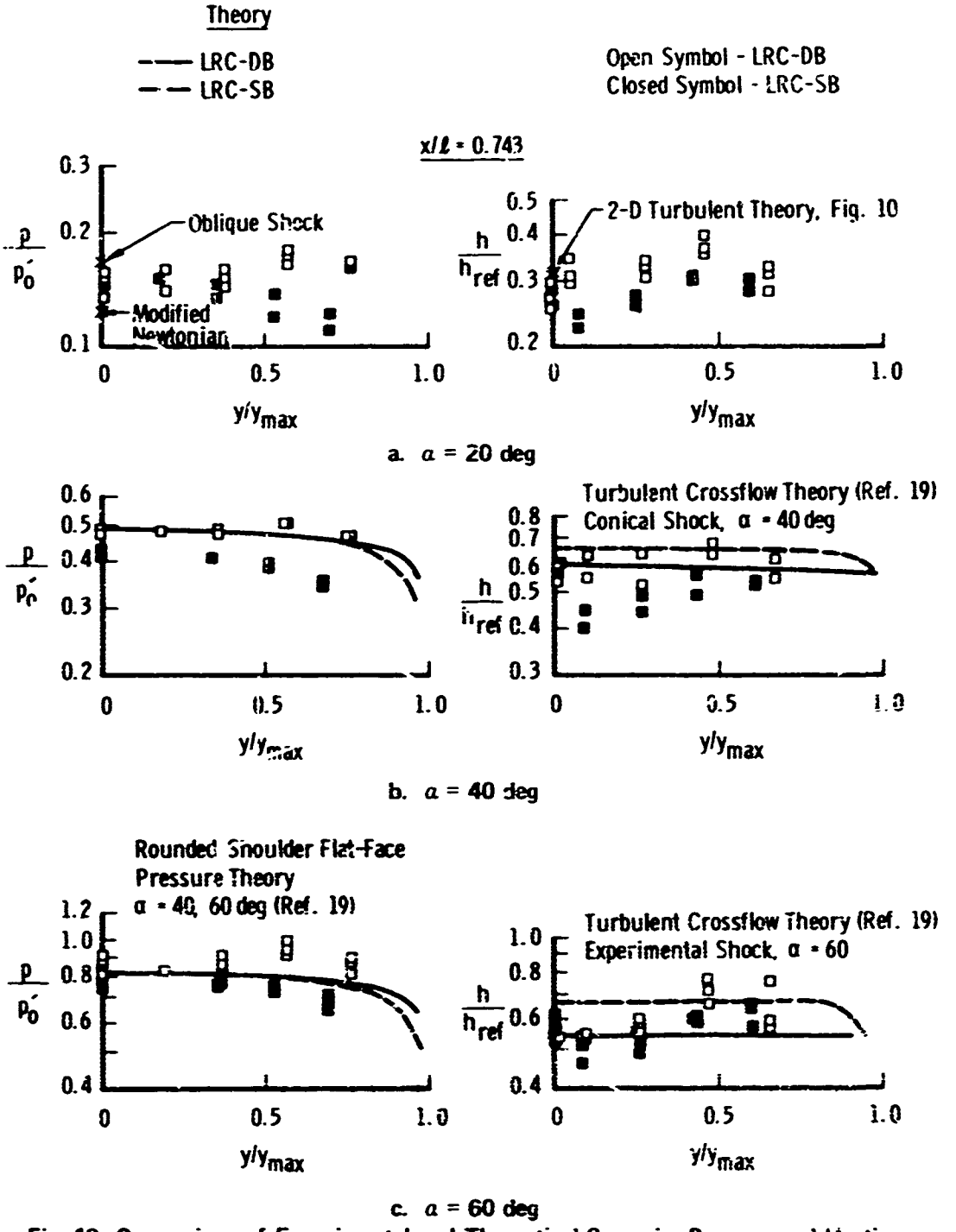

Fig. 13 Comparison of Experimental and Theoretical Spanwise Pressure and Heating Distributions at $M_\infty \approx 10.5$ and $Re_{\infty,\ell} \approx 10 \times 10^6$ (Tunnel F)

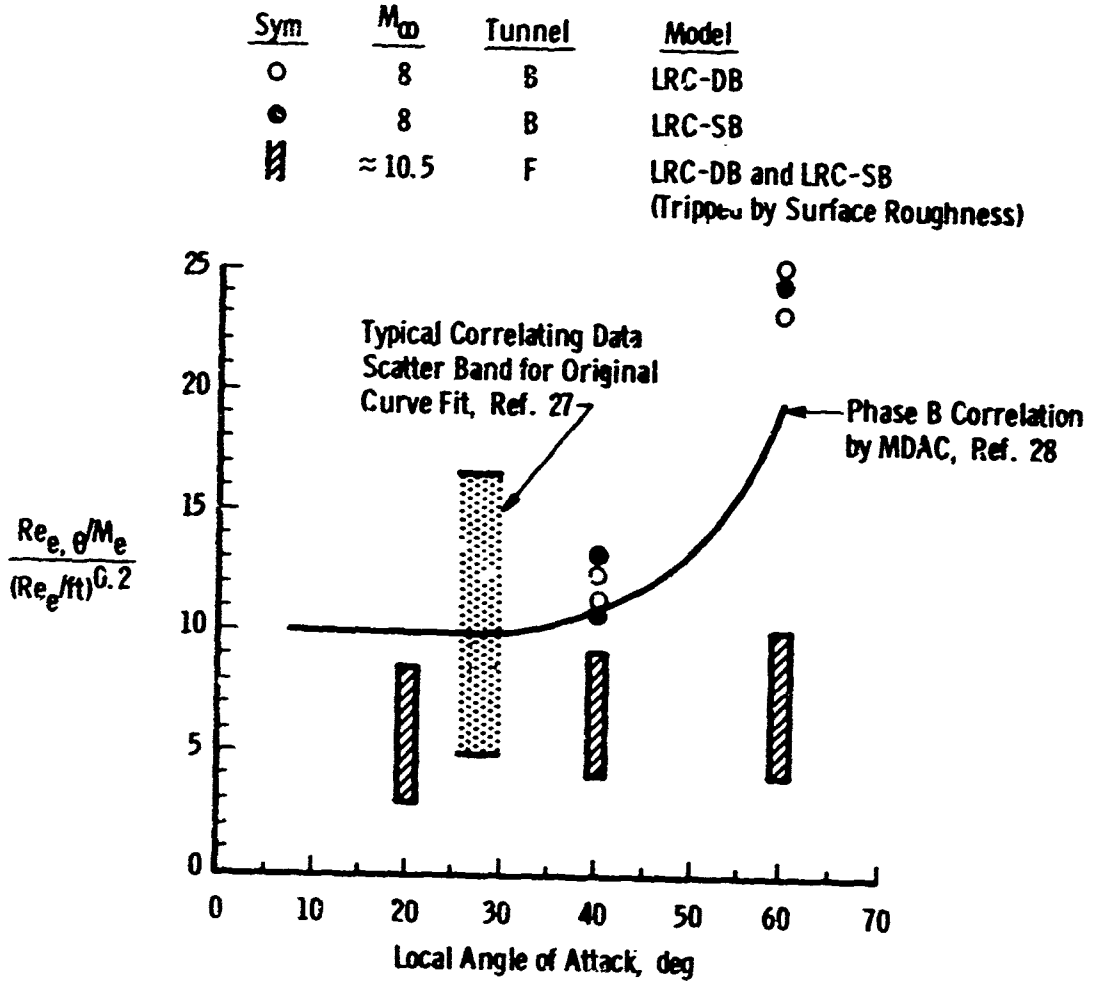

Fig. 14 Comparison of Transition Data with the Kipp-Masek Correlation

TABLE I
TEST SUMMARY OF NOMINAL TEST CONDITIONS

MODELS: LRC-DB and LRC-SB, ℓ = 24 in.

M_∞	p_o, psia	T_o, °R	Re_∞, ft^{-1} x 10^{-6}	$Re_{\infty,\ell}$ x 10^{-6}	h_{ref}, Btu/ft^2-sec-°R	α, deg	Type Data
8 (Tunnel B)	555, 860	1310, 1345	2.5, 3.7	5.0, 7.4	0.0221, 0.0277	20, 40, 60	P
~10.5 (Tunnel F)	2900 - 10,500	1660 - 2990	2.5 - 11.5	5 - 23	0.031 - 0.069	20, 40, 60	G, Ph, S, SP

NOTE: The maximum values of h_{ref} correspond to the maximum Reynolds number condition.

Data Code

G	Heat Gage
P	Phase Change Paint
Ph	Phosphor Paint
S	Schlieren
SP	Surface Pressure

TABLE II
TUNNEL CONDITIONS CORRESPONDING TO $M_\infty \approx 10.5$ (TUNNEL F) PLOTTED RESULTS

Run No.	Results	Figure	Figure Symbol	α, deg	M_∞	$Re_{\infty,\ell}$	p_∞, psia	ρ_∞, lbm/ft^3	U_∞, ft/sec	H_o, Btu/lbm	T_o, °R	p_o, psia	$p_{o'}$, psia	$\dot{q}_{ref}$, Btu/ft^2-sec	h_{ref}, Btu/ft^2-sec-°R
3631	Pressure	7, 10, 13	□	20	10.7	10.2×10^6	0.109	0.00261	5430	616	2280	5770	15.3	78.8	0.0454
3632	and Heat-				10.4	9.6×10^6	0.149	0.00280	6100	777	2810	7880	20.8	126.5	0.0557
3633	Transfer				10.3	10.5×10^6	0.100	0.00261	5130	550	2040	4760	13.7	63.7	0.0425
3646			■	20.2	10.5	10.2×10^6	0.102	0.00254	5360	598	2210	5570	14.5	73.2	0.0438
3647				*	10.2	9.9×10^6	0.119	0.00268	5490	629	2330	5520	16.1	83.3	0.0466
3634			□	40.2	10.3	9.1×10^6	0.121	0.00254	5740	689	2530	6100	16.7	97.7	0.0290
3635				40.5*	10.3	10.0×10^6	0.144	0.00286	5900	728	2650	7200	19.9	114.8	0.0544
3641			■	40.2	10.6	9.8×10^6	0.096	0.00241	5400	607	2250	5670	14.0	73.5	0.0431
3645					10.7	11.3×10^6	0.115	0.00283	5410	610	2250	6340	16.5	80.4	0.0471
3636			□	61.0	10.8	10.5×10^6	0.097	0.00251	5370	601	2220	6080	14.4	73.6	0.0439
3637				60.2	10.3	9.2×10^6	0.077	0.00220	4900	502	1860	3620	10.5	48.2	0.0366
3639				60.5*	10.6	10.2×10^6	0.124	0.00270	5800	702	2560	7460	18.1	104.5	0.0517
3642			■	60.2	10.6	9.8×10^6	0.104	0.00248	5520	636	2350	6040	15.1	81.9	0.0454
3648					10.7	10.2×10^6	0.094	0.00247	5330	591	2190	5700	13.9	70.4	0.0428
3649				60.5	10.4	10.3×10^6	0.141	0.00288	5890	723	2630	7500	19.3	113.8	0.0544
3635	Heat-	11	□	40.5*	10.6	22.1×10^6	0.183	0.00515	5080	539	1940	9440	26.5	84.7	0.0605
	Transfer		◗	*	10.3	11.2×10^6	0.154	0.00316	5810	705	2570	7600	21.2	113.7	0.0560
			◇	*	10.3	5.2×10^6	0.092	0.00161	6260	820	2990	4950	12.6	106.0	0.0433

*Free-Stream Conditions Used in Theoretical Boundary-Layer Calculations

TABLE III
TUNNEL F TEST MATRIX

Model	α, deg	Run	$\sim M_\infty$	$\sim Re_{\infty,\ell}$
LRC-DB	20.0	3631	10.4	7-13 x 10^6
	20.0	3632	10.5	7-21 x 10^6
	20.0	3633	10.4	7-15 x 10^6
	40.2	3634	10.4	6-14 x 10^6
	40.5	3635	10.4	5-22 x 10^6
	61.0	3636	10.8	9-22 x 10^6
	60.2	3637	10.4	5-9 x 10^6
	61.0	3638	10.6	9 x 10^6
	60.5	3639	10.6	10-20 x 10^6
LRC-SB	20.2	3646	10.6	10-18 x 10^6
	20.2	3647	10.3	6-18 x 10^6
	40.2	3541	10.7	7-16 x 10^6
	40.2	3645	10.6	11-23 x 10^6
	60.2	3642	10.6	5-10 x 10^6
	60.2	3648	10.6	10-20 x 10^6
	60.5	3649	10.5	6-17 x 10^6